

A method for 2-dimensional inversion of gravity data

Vatankhah, S.^{1*}, Ardestani, E. V.² and Ashtari Jafari, M.³

¹Ph. D. Student of Geophysics, Department of Earth Physics, Institute of Geophysics, University of Tehran, Iran

²Professor, Department of Earth Physics, Institute of Geophysics, University of Tehran, Iran

³Assistant Professor, Department of Earth Physics, Institute of Geophysics, University of Tehran, Iran

(Received: 12 Sep 2010, Accepted: 09 Oct 2012)

Abstract

Applying 2D algorithms for inverting the potential field data is more useful and efficient than their 3D counterparts, whenever the geologic situation permits. This is because the computation time is less and modeling the subsurface is easier. In this paper we present a 2D inversion algorithm for interpreting gravity data by employing a set of constraints including minimum distance, smoothness, and compactness. Using different combination of these constraints provide either smooth images of the underground geological structures or models with sharp geological boundaries. We model the study area by a large number of infinitely long horizontal prisms with square cross-sections and unknown densities. The final density distribution is obtained by minimizing an objective function that is composed of the model objective function and equality constraints, which are combined using a Lagrangian multipliers. Each block's weight depends on depth, a priori information on density and the allowed density ranges for the specified area. A MATLAB code has been developed and tested on a synthetic model consists of vertical and dipping dikes. The algorithm is applied with different combinations of constraints and the practical aspects are discussed. Results indicate that when a combination of constraints is used, the geometry and density distribution of both structures can be reconstructed. The method is applied on Zereshlu Mining Camp in Zanjan - Iran, which is well known for the Manganese ores. Result represents a high density distribution with the horizontal extension of about 30 m, and the vertical extension shows a trend in the E - W direction with a depth interval between 7 to 22 m in the east and 15 to 35 m in the west.

Keywords: Gravity, 2D inversion, Minimum distance, Smoothness, Compactness

1 Introduction

Gravity inversion recovers models of density distribution from data that are measured on finite discrete points on the Earth's surface. Following Gauss' theorem, there are many equivalent sources that can produce the same known field at the surface (theoretical ambiguity). Meanwhile, as the parameterization of problem is such that there are more unknowns than observations, the system does not provide enough information to uniquely determine model parameters (algebraic ambiguity). Although a density distribution which satisfies the observed data can be easily found, the non-uniqueness of the solution still exists. It is also obvious that measurements on the

Earth's surface cannot be carried carry out without errors that will impose arbitrarily large changes on the solution (instability of solution). Thus, the inversion of gravity data is a typical example of an ill-posed problem, so that it is necessary to include more information about the desired solution in order to find a geologically acceptable solution. The additional information can be divided into two groups: 1) a set of mathematical constraints that stabilize the problem and recover the model with certain criteria; and 2) the geological-based constraints which are added to produce reliable models consistent with geology. During last decades different authors have

*Corresponding author:

E-mail: svatan@ut.ac.ir

used several approaches to introduce a priori information into gravity inversion. Green (1975) found the closest model to the initial model, Last and Kubik (1983) minimized the volume of the causative body, Guillen and Menichetti (1984) concentrated the solution about a geometric element. Li and Oldenburg (1996, 1998) counteracted the decreasing sensitivity of the cells with depth by weighting it with an inverse function of depth. Smoothness or roughness of physical parameters distribution that control gradients in spatial direction used by Pilkington (1997) and Li and Oldenburg (1996, 1998). Boulanger and Chouteau (2001) employed a 3D inversion algorithm that implements several constraints, including minimum distance, flatness, smoothness and compactness.

Gravity inversion can be carried out either in the two or three dimensional spaces, depending on the type of problem to be tackled. Therefore, the first question to be raised is whether to use a two or three dimensional gravity inversion to fully recover the location, shape and density of the sources. Two-dimensional methods are suitable to be applied on the geological structures such as faults, dikes and rift zones over which the length of the source body (y-direction) is much longer than its width in x and z directions. Then, it may be possible to consider the gravitational sources as completely invariant in the direction parallel to the length direction. Additionally, 2D sources are easier to conceptualize and

considerably easier to be modeled than their 3D counterparts (Blakely, 1996).

In this paper a 2D version of the Boulanger and Chouteau's (2001) 3D method is developed. First, the subsurface under the gravity profile is divided into a large number of infinitely long horizontal prisms with square cross-sections, which density for each block is an unknown constant. Later, an analytical calculation for the model is derived. To solve the inverse problem, weighted model objective function and equality constraints are combined. Tests are performed using different combinations of constraints on synthetic model. Finally, as a practical application the method is applied on a profile of gravity data gathered from Zereshlu mining camp.

2 Gravity modelling

The subsurface under the survey area is divided into a large number of infinitely long horizontal prisms, with square cross-section and unknown densities (Figure 1). This type of parameterization is a simple two-dimensional modeling. The y axis is directed parallel to the invariant direction and variations in densities are only allowed for the x and z directions. The cross-section of the model under gravity profile is shown in Figure 2. The cells are square and their dimensions are equal to the distance between two observation points. Here the unknown density is considered to be constant for each block and the data and model parameters are linearly related.

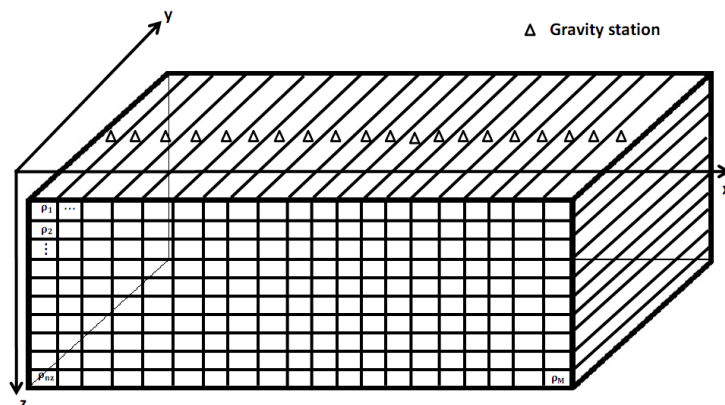


Figure 1. Discretization of the subsurface with infinity long horizontal prisms.

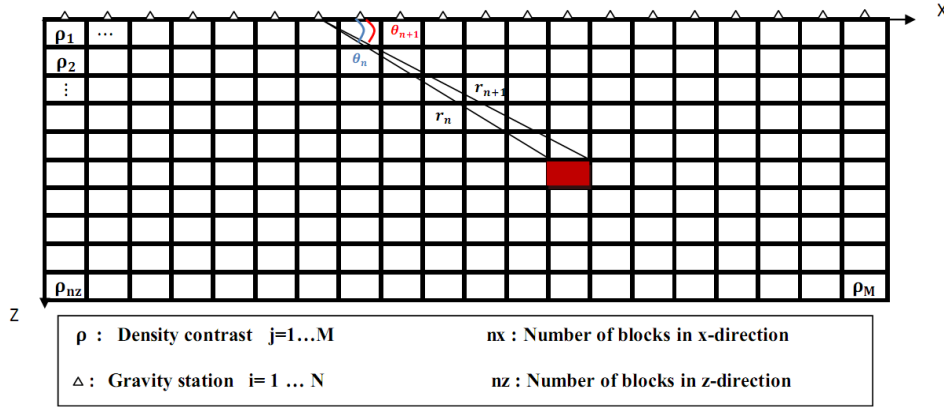


Figure 2. Cross-section of the model under gravity profile. Gravity stations are located at the center of the blocks at the ground surface. Cells are square and their dimensions are equal to the distance between two observation points.

The vertical component of the gravitational attraction of a two-dimensional body at the origin using Cartesian coordinate system is given by Blakely (1996):

$$g_i = 2\gamma\rho \iint \frac{z'dx'dz'}{x'^2+z'^2} \quad (1)$$

Here γ is the universal gravitational constant and the density ρ is assumed to be constant within the body. A solution of this integral for L-sided polygon is given by Blakely (1996):

$$\frac{g_i}{\rho} = 2\gamma \sum_{n=1}^L \frac{\beta_n}{1+\alpha_n^2} \left[\log \frac{r_{n+1}}{r_n} - \alpha_n (\theta_{n+1} - \theta_n) \right] \quad (2)$$

where $\alpha_n = \frac{x_{n+1} - x_n}{z_{n+1} - z_n}$ and $\beta_n = x_n - \alpha_n z_n$.

In Figure 2, r_n , r_{n+1} , θ_n and θ_{n+1} are displayed for the upper side of a square block. The term on the right-hand side of the equation (2) quantifies the contribution to the i th datum of a unit density in the j th cell (G_{ij}). This response is valid only at the station i and for one prism. To obtain the total response at each station i , the gravity responses of M prisms are summed:

$$g_i = \sum_{j=1}^M G_{ij} \rho_j \quad i=1 \dots N \quad (3)$$

Geophysical data always contaminated with noise, thus equation (3) in matrix notation is:

$$\mathbf{g} = \mathbf{G}\boldsymbol{\rho} + \mathbf{e} \quad (4)$$

G is the forward operator matrix or kernel that maps from the physical parameter space to the data space and \mathbf{e} is N -dimensional vector represents errors in the measurements.

3 Inversion methodology

Green (1975), based on Backus and Gilbert (1967) approach, proposed a linear method for inversion of gravity data. The approach uses the minimization of a cost functional that consists of the weighted distance of an acceptable model from an initial state, subject to an equality constraint, which can be solved using Lagrangian multipliers (See appendix A). Boulanger and Chouteau (2001) used Green's method and developed a three-dimensional inversion algorithm to interpret gravity data using a set of constraints. Following their method, the Lagrangian function is given by

$$L(\boldsymbol{\rho}, \boldsymbol{\theta}) = \frac{1}{2} (\boldsymbol{\rho} - \boldsymbol{\rho}^0)^T \mathbf{W}^T \mathbf{W} (\boldsymbol{\rho} - \boldsymbol{\rho}^0) + (\mathbf{b} - \mathbf{A}(\boldsymbol{\rho} - \boldsymbol{\rho}^0))^T \boldsymbol{\theta} \quad (5)$$

This objective function is flexible and allows inserting various constraints and a priori information in the inversion process. It is composed of:

$$\mathbf{A} = \begin{bmatrix} \mathbf{G} \\ \mathbf{H} \end{bmatrix}_{(N+M) \times M} \quad (6)$$

Here $G_{N \times M}$ is the forward operator matrix and $H_{M \times M}$ is the first or the second derivative matrices (∂ or ∂^2) that multiplied by $\boldsymbol{\xi}_H$ ($\boldsymbol{\xi}_H \partial$)

or $\xi_H \partial^2$). The coefficient ξ_H gives either more or less importance to the matrix H . The first and second derivatives are referred to ‘flatness’ and ‘smoothness’ constraints respectively, which have two effects in the inversion process. Firstly, they produce flat or smooth density distribution and secondly they improve the numerical stability of inversion by preventing unlimited growth of a single parameter. In this paper smoothness constraint is used such that for 2D structure according to Figure 2 we need to constitute $\zeta_{H_x} \partial_x^2 + \zeta_{H_z} \partial_z^2$. The ∂_x^2 and ∂_z^2 matrices represent the finite-difference approximation to taking model derivatives in x and z directions. Considering that the grid consists of M parameters with nx elements in the x -direction and nz elements in the z -direction (elements are numbered up to down starting at the top left element). The $M \times M$ matrices of ∂_z^2 and ∂_x^2 are given by:

$$\partial_z^2 = \begin{bmatrix} 1 & -2 & 1 & & & \\ & 1 & -2 & 1 & & \mathbf{0} \\ & & \ddots & & & \\ & \mathbf{0} & & & 1 & -2 & 1 \\ & & & & & 1 & -2 & 1 \end{bmatrix} \quad (7)$$

$$\partial_x^2 = \begin{bmatrix} 1 & \mathbf{0} & -2 & \mathbf{0} & 1 & & & & & \\ & & 1 & \mathbf{0} & -2 & \mathbf{0} & 1 & & & \\ & & & \ddots & & \ddots & & \ddots & & \\ & & & & & & & & 1 & \mathbf{0} & -2 & \mathbf{0} & 1 \\ & & & & & & & & 1 & \mathbf{0} & -2 & \mathbf{0} & 1 \end{bmatrix} \quad (8)$$

Here $\mathbf{0}$ in the rows of ∂_x^2 is a vector contains $nz - 1$ zero.

$$\mathbf{b} = \begin{bmatrix} \Delta \mathbf{g} \\ \mathbf{0} \end{bmatrix}_{(N+M) \times 1} \quad (9)$$

where $\Delta \mathbf{g}_{N \times 1}$ is the difference between the observed and the calculated anomaly ($\mathbf{g}^{obs} - \mathbf{g}^{pre}$) and $\mathbf{0}_{M \times 1}$ is the null vector.

$$\boldsymbol{\theta} = \begin{bmatrix} \boldsymbol{\alpha} \\ \boldsymbol{\zeta} \end{bmatrix}_{(N+M) \times 1} \quad (10)$$

where $\boldsymbol{\theta}$ is a Lagrange multiplier associated with equality constraints and splits into $\boldsymbol{\alpha}$ for $\Delta \mathbf{g}$ and $\boldsymbol{\zeta}$ for $\mathbf{0}$.

$\boldsymbol{\rho}^0$ is the vector contains initial contrasts of density. Normally $\boldsymbol{\rho}^0 = \mathbf{0}$, but if a priori

knowledge of the properties of the subsurface distribution exists, a full model of the expected physical properties could be used.

$W_{M \times M} = P^{-1} Q V$ consists of three diagonal matrices P , Q and V .

P is the matrix of the ‘hard’ constraint, where P_{jj} is fixed at $\eta = 10^{-2}$ when geological information provides the value of initial density of the j th cell (ρ_j^0), otherwise P_{jj} is fixed at 1. Moreover, in this algorithm positivity of densities is imposed during the inversion by cutting out densities beyond the allowable bounds, $([\rho_{min}, \rho_{max}])$, and resets them to these limits.

Q is the depth weighting matrix with diagonal elements $Q_{jj} = \frac{1}{(z_j + \sigma)^\beta}$ which was

introduced by Li and Oldenburg (1996, 1998) and Pilkington (1997), (z_j is the mean depth of the cell j and σ is a small number to avoid singularity at the surface). It is obvious that amplitudes of kernel rapidly diminish with depth, then during the inversion process reconstructed models tend to concentrate near the surface regardless of the true depth of the causative bodies. Using depth weighting matrix counteracts the natural decay of the kernel, so that all cells have an equal probability during the inversion. The weight depends on power β , which small values of β result shallow reconstruction for solution, while large values concentrate the solution at depth, implying that it is important to choose an acceptable value for β . We illustrated the effect of different values of parameter β on inversion of gravity data for a square. The square has the dimension of 40×40 m and buried at a depth of 10 m (Figure 3a). The density of the square is 0.5 g/cm^3 . Synthetic data are calculated on a profile including 50 stations of 10-m spacing. We added Gaussian noise with zero mean and standard deviation 5% of the maximum datum. The subsurface is divided into 500 cells (50 cells in x -direction and 10 cells in z -direction). Objective function of equation (5) with depth

weighting, positivity and smoothness (without compactness constraint) is used for $\beta=0, 0.9, 1.4$ and results are shown in Figures 3b-d, respectively. For $\beta=0$ reconstructed model tends to concentrate near the surface, while for $\beta=1.4$ it tends to be deeper. For $\beta=0.9$ inversion algorithm tends toward intermediate depths and gives reasonable results. However, 0.9 is not the only value for β and in our test an acceptable range of $[0.6 \ 1]$ was found for this parameter.

V is a minimum area (compactness) constraint with diagonal elements $V_{jj} = \frac{1}{\rho_j^2 + \varepsilon}$.

This constraint which was introduced by Last and Kubik (1983) seeks to minimize the area (in 2D) or volume (in 3D) using density of each block as weight. As this weighting matrix does not penalize sharp or blocky features, it is a suitable constraint for geologic structures such as faults, dikes or cavities which have properties that are relatively localized within the area under consideration. This concept is further developed by Portniaguine and Zhdanov (1999) who used term “minimum support”. The parameter ε is a small number which is introduced to provide stability as $\rho_j \rightarrow 0$. It plays very important role in compactness constraint. In general, we are interested

in the case where $\varepsilon \rightarrow 0$, though there are practical limitations because its small value leads to very compact models and increases instability of the solution. Meanwhile, if ε is chosen large, this constraint has no influence on compactness of the model. Figure 4 shows the compactness term of the objective function in equation (5), $\phi = \rho^T W^T W \rho$, as a function of ε (without depth weighting and hard constraint, i.e. $W=V$ and with $\rho^0=0$). As ε becomes smaller, the notch near zero becomes sharper (Figure 4), indicating that the model parameters values should drop below this level in order to reduce the compactness term in the objective function. Conversely, as ε becomes large, it acts like a weighted minimum length constraint and will lose its property.

A trade-off curve method is usually used to select ε by computing model objective function for the current model estimate over a range of values for ε (Minsley et al., 2006). The optimal value is chosen at the point of maximum curvature on a log-log plot (Figure 5). This value of ε is then used to compute a new model estimate. This ensures that inversion stability is maintained while the value of the objective function does not deviate strongly from its value when $\varepsilon = 0$.

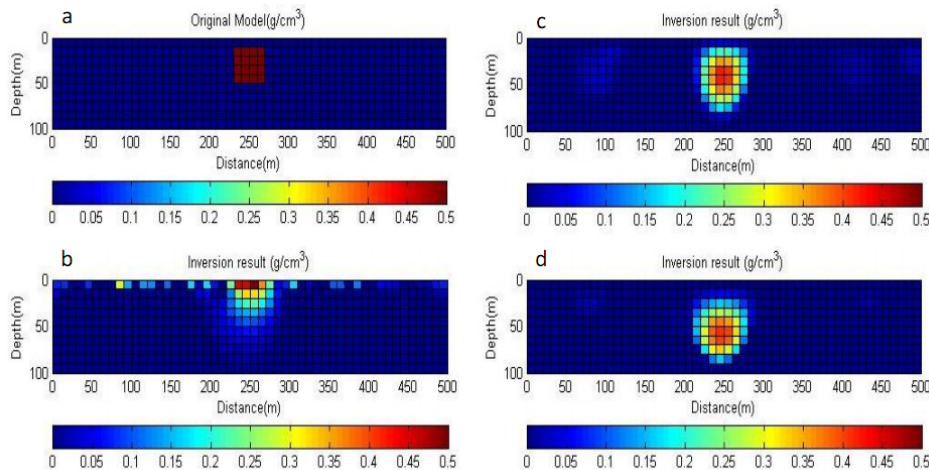


Figure 3. (a) Illustration of the effect of the depth weighting function. Original model is square with the dimensions of 40×40 m. (b), (c) and (d) display inversion results for $\beta=0, 0.9$ and 1.4 , respectively.

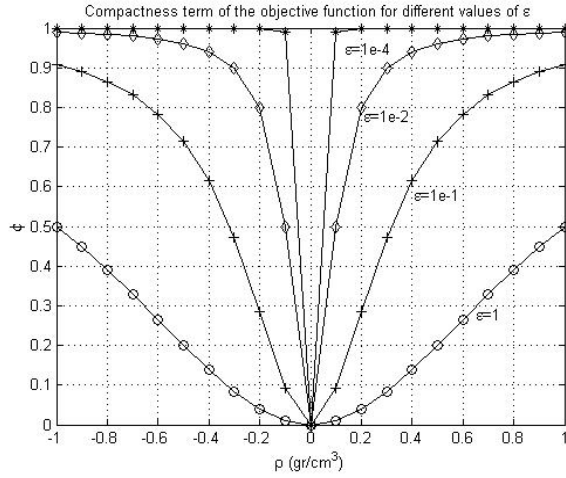


Figure 4. Comparison of the compactness term in the objective function for different values of \mathcal{E} .

Minimization of the objective function of equation (5), $L(\rho, \theta)$, with respect to ρ and θ gives a system of two equations:

$$(AW^{-1})(AW^{-1})^T \theta^k = b^k \tag{11}$$

$$\rho^{k+1} = \rho^k + W^{-1}(AW^{-1})^T \theta^k \tag{12}$$

as W is not constant, the computational procedure is an iterative approach. For the first implementation of the algorithm, matrices P and V are chosen equal to identity matrix. For the next iterations, minimum area matrix is a function of the previous estimate of the model parameters, $V_{jj}^k = \frac{1}{\rho_{j^{(k-1)}}^2 + \mathcal{E}}$, and hard constraint

matrix is adjusted according to the style mentioned above. At each iteration, a solution for θ^k is computed from equation (11), and this θ^k is then replaced into

equation (12) to give the solution ρ^{k+1} . The anomaly g^{k+1} and the vector Δg^{k+1} are calculated to estimate $\chi^2 = \left\| \frac{g_i^{obs} - g_i^{cal}}{\sigma_i} \right\|_2^2$

magnitude (σ_i is the error standard deviation). The program stops when the solution reaches the noise level, $\chi^2 \leq N + \sqrt{2N}$, or a maximum number of iterations. In the present paper, the inverse matrix calculation in equation (11), $((AW^{-1})(AW^{-1})^T)^{-1}$, is done by truncated singular value decomposition (TSVD). TSVD is a well-known and numerically stable method for dealing with ill-condition matrices and is a standard tool for small inverse problems. The basic idea of TSVD is to neglect the component of the solution corresponding to the smallest singular values. A complete detail about TSVD is given in Hansen (1987).

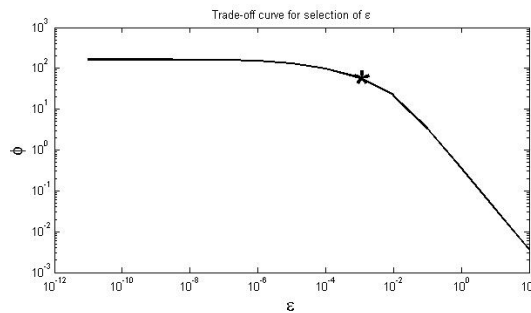


Figure 5. Trade-off curve that illustrates the selection of \mathcal{E} for the compactness constraint.

4 Synthetic model

The forward modeling and the inversion code have been developed using MATLAB. For testing the validity of the program and the inversion method, we invert the gravity data which was produced by synthetic model consisting of dipping and vertical dikes. Figure 6 shows this model and its gravity anomaly. The bodies have various depth and size, while density contrast for both models are the same. Data are calculated at 50 stations with 10-m spacing, and the Gaussian noise with zero mean and standard deviation 5% of the maximum datum is added.

At the first step, the inversion is done using minimum distance and smoothness constraints. The starting model for inversion is a homogeneous ground with density of $\rho_0=0$. The subsurface is divided into $50 \times 10 = 500$ cells, with cell size of 10 m. Here the density limits are set to $0 \text{ g/cm}^3 \leq \rho \leq +0.5 \text{ g/cm}^3$. The coefficient β in depth weighting matrix is chosen 0.85. To

illustrate the application of smoothness constraints, the algorithm is implemented with two values of ζ_H (i.e. $\zeta_{H_x} = \zeta_{H_z} = 0.01$ and $\zeta_{H_x} = \zeta_{H_z} = 0.03$). The inversion results are presented in Figure 7. In both cases the depth to the top of the bodies are close to those of the original model, but the slope of the dipping dike in the first case is recovered better than the second case. In Figure 7a, density values of maximum 0.5 g/cm^3 for dipping dike and 0.4 g/cm^3 for vertical dike are found, while in Figure 7b they are 0.5 g/cm^3 and 0.3 g/cm^3 , respectively. Results show that with increasing smoothness the density distribution tends to spread in more cells, while the magnitude of obtaining parameters decreases. It should be mentioned that smoothness preserves smooth images of the underground geological structures and avoids models with sharp geological boundaries for which the degree of smoothness is related to ζ (see Figure 7).

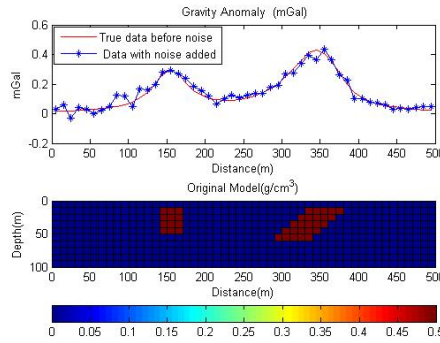


Figure 6. The synthetic model that used to test the inversion method. Contrast of densities for dipping and vertical dikes are 0.5 g/cm^3 . Gaussian noise with a zero mean and the standard deviation of 5% for the maximum datum is added.

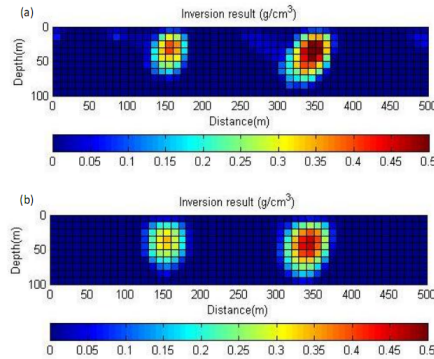


Figure 7. The density model obtained by inverting the gravity data of Figure 6 using minimum distance and smoothness constraints. Smoothness constraint is used in (a) with $\zeta_{H_x} = \zeta_{H_z} = 0.01$ and (b) with $\zeta_{H_x} = \zeta_{H_z} = 0.03$.

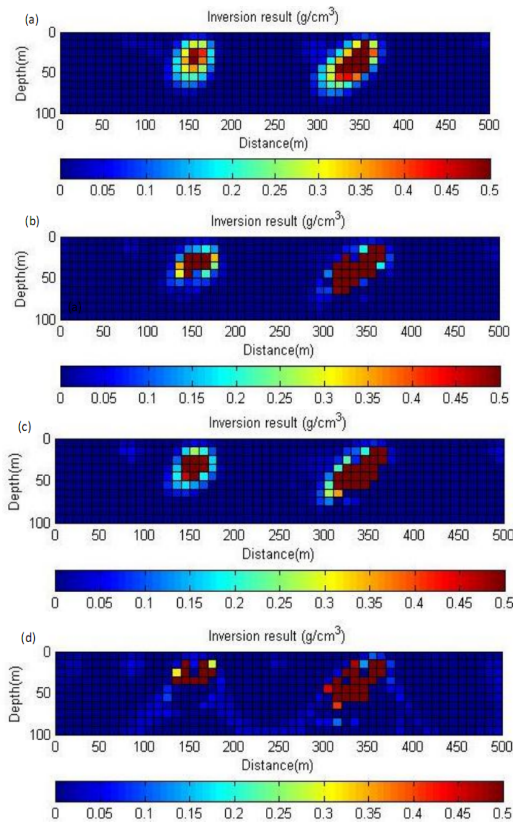


Figure 8. The density model obtained by inverting the gravity data of Figure 6 using minimum distance and compactness constraints for different values of ε . In (a), (b) and (d) the value of ε is 10^{-1} , 10^{-2} and 10^{-11} , respectively, while in (c) ε was chosen according to the trade-off curve method.

Second inversion is done using minimum distance and compactness constraints. The starting model for inversion is similar to the previous case with $\beta = 0.85$ and density limits are chosen to be 0 and 0.5 g/cm^3 . Tests are made using different values of parameter ε and results are shown in Figure 8. For $\varepsilon = 0.1$, we find a good reconstruction for both structures but the inversion does penalize sharp boundaries and tends to provide smooth solutions for structures. The maximum density value of 0.5 g/cm^3 is found for both bodies. For $\varepsilon = 0.01$, geometry and density of structures are better reconstructed, especially for dipping dike. Results show that by decreasing the value of ε , the inversion can resolve the structures with sharp boundaries. Figure 8c shows the reconstructed density model for values of ε

which was computed according to the trade-off curve method. These values are usually in the range of $10^{-2} - 10^{-3}$, suggesting that the result is very close to the case (b). In Figure 8d, the inversion result using $\varepsilon = 10^{-11}$ is shown. As expected, the sources become more compacted and the amplitude of sources increases by increasing compactness in order to fit the data.

The last inversion uses combination of three constraints, i.e. minimum distance, smoothness and compactness. In this stage, parameter ε is chosen according to the trade-off curve method and inversion is done for different values of ζ_H . Results are shown in Figure 9 for $\zeta_{H_x} = \zeta_{H_z} = 0.01$ and $\zeta_{H_x} = \zeta_{H_z} = 0.07$. The reconstructed models in Figures 7, 8 and 9 illustrate the effect of using combination of these constraints with choosing suitable values of parameters ε and ζ_H . The last inversion seems to best recover the geometry and density values for the sources; especially the slope of the dipping dike is well recovered.

5 Real data

For applying the inversion on real data, we choose a profile of gravity data acquired over the Zereshlu Mining Camp, in Zanjan-Iran, well known for the Manganese ores. The area of the gravity survey extends between UTM coordinates [704296 704554] East and [4130627 4130990] North, zone 38. The area is covered by altered red Andesite with ferrous Oxide and Olivine Pyroxene Basalt Tuff, which the two structures are separated by a north-south fault (Figure 10).

Gravity survey was performed by gravity branch of the institute of Geophysics, University of Tehran. The measurements were corrected for effects caused by variation in latitude, elevation and topography to yield Bougure gravity anomaly. The residual anomaly is obtained by subtracting the regional anomaly from Bouguer anomaly using polynomial fitting method (Figure 11). A profile of the residual anomaly (AA') consisting of 26 data measurements, sampled every 2.5 m, is chosen for inversion. We have assigned each datum an error whose

standard deviation is 2% of its magnitude. The subsurface is divided into $26 \times 20 = 520$ cells of side 2.5 m. Based on a priori information, background density of 2.6 g/cm^3 and density limits of $[2.5 \text{ g/cm}^3 \text{ } 3.3 \text{ g/cm}^3]$ are chosen for the inversion. Inversion is carried out with a combination of minimum distance, smoothness and minimum area constraints for which $\beta = 0.85$ and $\zeta_{H_x} = \zeta_{H_z} = 0.01$ are

chosen. Figure 12 displays the recovered density model from the inversion of profile AA' which clearly represents the density contrast and geometry for manganese ore occurrence. The horizontal extension of the obtained model is about 30 m and the vertical extension shows a trend in the E-W direction with a depth interval between 7 to 22 m in the east and 15 to 35 m in the west.

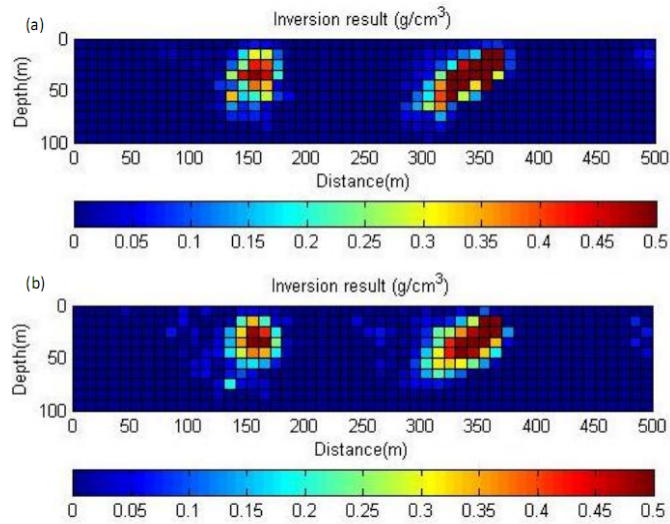


Figure 9. The density model obtained by inverting the gravity data of Figure 6 using minimum distance, smoothness and compactness constraints. The parameter ε is chosen according to the trade-off curve method and inversion is done for (a) $\zeta_{H_x} = \zeta_{H_z} = 0.01$ and (b) $\zeta_{H_x} = \zeta_{H_z} = 0.07$.

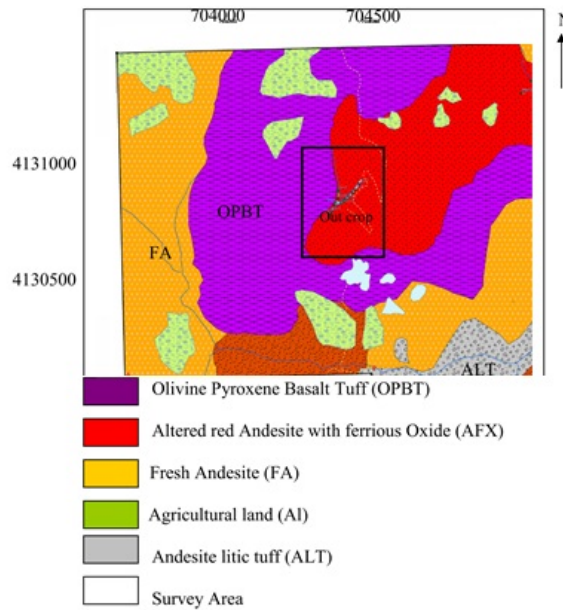


Figure 10. Geological map of the Zereshlu Mining Camp.

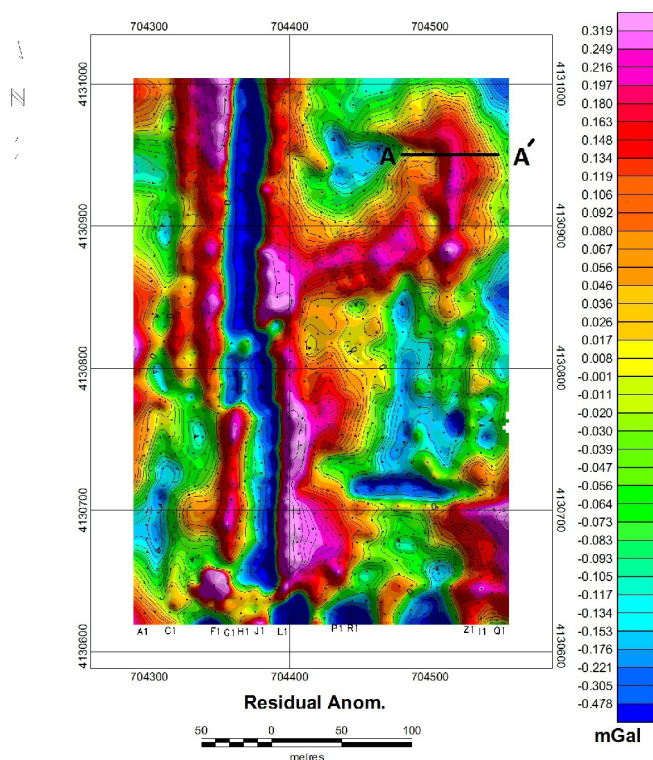


Figure 11. The residual anomaly over the Zereshlu mining camp.

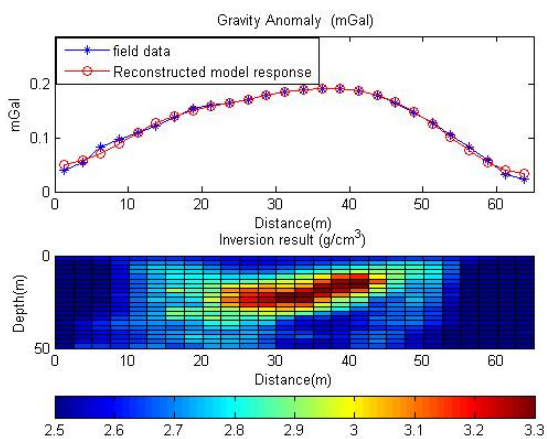


Figure 12. The density model obtained by inverting field gravity data (profile AA'). The subsurface is divided into $26 \times 20 = 520$ cells of side 2.5 m. The density contrast and the geometry for manganese ore occurrence well recovered.

6 Conclusion

We have developed a 2D inversion algorithm based on available 3D algorithm proposed by Boulanger and Chouteau (2001). The algorithm is flexible and allows inclusion of

minimum distance, smoothness and compactness constraints. Density limits and depth weighting can also be integrated into the algorithm. The practical aspects of the application of these constraints and effective parameters have been discussed. The inverse matrix calculation was done by truncated singular value decomposition which is a suitable method for small inverse problems. We tested the algorithm on a synthetic model consisting of dipping and vertical dikes. Different constraints were applied individually or in combination with each other. In all cases, the geometry and density for model well recovered, although combination of minimum distance, smoothness and compactness provide better results. The developed method allows the user to employ smoothness or compactness constraints separately. We applied the algorithm on a gravity profile measured at the Zereshlu Mining Camp. The result represents a high density distribution with the horizontal extension of about 30 m and the vertical extension shows a trend in the E-W

direction with a depth interval between 7 to 22 m in the east and 15m to35m in the west.

Appendix

Derivation of the inversion algorithm

We wish to find a model ρ which has two properties:

1) Satisfies the observed gravity data (\mathbf{g}^{obs}), i.e,

$$\mathbf{g}^{pre}(\rho) = \mathbf{g}^{obs} \quad (A-1)$$

Here $\mathbf{g}^{pre}(\rho)$ are the gravity values predicted by the model parameter ρ .

2) It should be closest to an initial estimate of parameters, ρ^0 . In the parameter space, the distance of ρ from ρ^0 is given by $\|\rho - \rho^0\|_2^2 = (\rho - \rho^0, \rho - \rho^0)$. In addition, we want to consider weighting factor W applied to each cell in the model. The weighted distance of an acceptable model from an initial guess becomes

$$\|W(\rho - \rho^0)\|_2^2 = (W(\rho - \rho^0), W(\rho - \rho^0)) \quad (A-2)$$

relation between \mathbf{g} and the model parameter ρ is linear:

$$\mathbf{g}^{pre}(\rho) = (G, \rho) \quad (A-3)$$

Where G is the kernel and (G, ρ) denotes an inner product. The gravity effect of the initial model is

$$\mathbf{g}^{pre}(\rho^0) = (G, \rho^0) \quad (A-4)$$

from (A-1), (A-3) and (A-4), we have:

$$\mathbf{g}^{obs} - \mathbf{g}^{pre}(\rho^0) = G(\rho - \rho^0) \quad (A-5)$$

The problem is then to minimize $\|W(\rho - \rho^0)\|_2^2$ subject to the constraints $\mathbf{g}^{obs} - \mathbf{g}^{pre}(\rho^0) = G(\rho - \rho^0)$ which can be solved using Lagrangian multipliers:

$$\frac{1}{2} \|W(\rho - \rho^0)\|_2^2 + (\Delta \mathbf{g} - G(\rho - \rho^0))^T \theta \quad (A-6)$$

References

- Backus, G. and Gilbert, J. F., 1967, Numerical applications of a formalism for geophysical inverse problems, *Geophysical Journal of the Royal Astronomical Society*, **13**, 247-276.
- Blakely, R. J., 1996, *Potential theory in gravity & magnetic applications*, Cambridge University Press.
- Boulianger, O. and Chouteau, M., 2001, Constraints in 3D gravity inversion, *Geophysical Prospecting*, **49**, 265-280.
- Green, W. R., 1975, Inversion of gravity profiles by use of a Backus-Gilbert approach, *Geophysics*, **40**, 763-772.
- Guillen, A. and Menichetti, V., 1984, Gravity and magnetic inversion with minimization of a specific functional, *Geophysics*, **49**, 1354-1360.
- Hansen, P. C., 1987, The truncated SVD as a method for regularization, *BIT*, **27**, 543-553.
- Last, B. J. and Kubik, K., 1983, Compact gravity inversion, *Geophysics*, **48**, 713-721.
- Li, Y. and Oldenburg, D. W., 1996, 3D inversion of magnetic data, *Geophysics*, **61**, 394-408.
- Li, Y. and Oldenburg, D. W., 1998, 3D inversion of gravity data, *Geophysics*, **63**, 109-119.
- Minsley, B. J., Ajo-Franklin, J. B. and Morgan, F. D., 2006, *Non-linear constraints with application to self-potential source inversion*, Massachusetts Institute of Technology. Earth Resources Laboratory
- Pilkington, M., 1997, 3D magnetic imaging using conjugate gradients, *Geophysics*, **62**, 1132-1142.
- Portniaguine, O. and Zhdanov, M. S., 1999, Focusing geophysical inversion images, *Geophysics*, **64**, 874-887.